CrossMark

Application of the singularity mapping technique to identify local anomalies by polarization data (a case study: Hamyj Copper Deposit, Iran)

Mohammad Shahi Ferdows[1] · Hamid Reza Ramazi[1]

Abstract Separating anomalies plays a critical role on mineral exploration. In this paper, IP anomalies have been determined by concentration-area (C-A) and singularity methods. Then a comparison has been made between the methods. The singularity map (as well as fractal method) is usually applied in the geochemical exploration process; however, it has not been widely used in the geoelectrical methods so far. In this research, it has been successfully applied to utilize this method to process IP data (recognize anomaly induced polarization data in Hamyj copper deposit). Hamyj deposit is located about 80 km west of Birjand city, South Khorasan province, Iran. In this area, resistivity and induced polarization data have been surveyed by dipole-dipole array. Finally, according to the mentioned method, 67 % of the anomalies (singularity index) are confirmed by the concentration-area method which showed significant adaption with each other. Also, a suitable area is determined by a singularity map for drilling.

Keywords Fractal · Concentration-area · Singularity map · Induced polarization

1 Introduction

The most significant component of a mineral exploration program is to define and separate anomalous value from the background values (Bai et al. 2010). Statistical analysis methods such as probability plot, gap statistic, and analysis of variance play an important role in separating anomalous value from background (Sinclair 1974, 1976, 1991; Stanley and

✉ Hamid Reza Ramazi
  ramazi@aut.ac.ir

  Mohammad Shahi Ferdows
  m.shahi@aut.ac.ir

[1] Department of Mining & Metallurgical Engineering, Amirkabir University of Technology, Tehran, Iran

Sinclair 1989; Govett et al. 1975). These methods ignore spatial information and spatial autocorrelation structure of data. However, there are statistical methods in which the spatial structure of data can be taken into account, such as the moving average method, factor analysis, and etc. (Grunsky and Agterberg 1988). These methods have been highly applied in geochemical analysis; however, they have not been used in geophysical analysis as much as geochemical analysis.

The concept of fractal models were initially proposed by Mandelbrot (1967) about a half century ago (Xiao et al. 2012). Fractal and multi-fractal models have also been applied to separate anomalies from background. These models include the concentration-area model (C-A), spectrum-area model (S-A), multi-fractal singular value decomposition (MSVD), concentration-distance model (C-D) mapping singularity technique, and etc. (Zuo et al. 2009).

Various papers have been written based on the application of fractal models on different fields such as ocean, climatic and geophysical flow dynamics, etc. (Scholz and Mandelbrot 1992; Barton and La Pointe 1995a, b; Dhu et al. 1999).

These separation methods have been vastly used in geochemical data. In addition, this can create an innovative method to separate anomalies from background in geophysical interpretation as well as geochemical data processing. One of the important subset of geoelectrical exploration is IP method that is widely used in exploration mineral, etc. (Khalid and Ghazi 2013; Telford et al. 1990). In this paper, anomalies data were determined by a singularity map and a comparison has been made by the concentration-area method. 67 % of anomalies data corresponded with each other.

1.1 Singularity map

The concept of singularity has been used to characterize the anomalous behaviors of singular physical processes that often result in anomalous amounts of energy release or material accumulation within a narrow spatial–temporal interval (Cheng 2006, 2007, 2008). From a multifractal point of view, the singularity phenomenon in three-dimensional space can be described as a power-law relationship between volumes V in a mineralization domain and total amount of metal $\mu(V)$ as follows (Cheng 2007).

$$\mu(V) \propto V^{\frac{\alpha}{3}} \tag{1}$$

where $\propto$ denotes Proportion and α is the singularity index Because the metal concentration C(V) in V can be expressed as $C(V) = \frac{\mu(v)}{v}$, we also have:

$$C(V) \propto V^{\frac{\alpha}{3}-1} \tag{2}$$

For a two-dimensional situation, volume V is replaced by area A and volumetric concentration becomes areal concentration. Consequently, Eqs. 1 and 2 become (Cheng 2007).

$$\mu(A) \propto A^{\frac{\alpha}{2}} \tag{3}$$

$$C(A) \propto A^{\frac{\alpha}{2}-1} \tag{4}$$

The distribution of the singularity α in the mapped area can be described by the fractal dimension spectrum function f(α) which implies that for a conservative field the majority of the area has values of α that are close to 2, whereas the areas with values $\alpha > 2$ or $\alpha < 2$ are more irregular or unusual. (Cheng 2007, 2008). If values related to concentration of the

element are considered as realizations of a stationary random variable with a constant population mean, $\alpha \approx 2$ represents non singularity. "Singular" locations presented by $\alpha < 2$, determine enrichment of the element and those with $\alpha > 2$ indicate the depletion of the element. Further discussion of the existence and property of singularity can be found in (Cheng 2007, 2008).

A window-based method can be used to estimate the local singularity from a geochemical map (Cheng 2006, 2007). It can be described as follows:

– Giving a location on the map,
– Define a set of sliding windows A(r) (with square, circular, rectangular, or other shapes) with variable window sizes, $r_{min} = r_1 < r_2 < \cdots < r_n = r_{max}$,
– and
– Calculate the average concentration value $C[A(r_i)]$ for each window size. There should be a linear relationship between $C[A(r_i)]$ (i = 1,…, n) and r_i, or

$$\log C[A(r_i)] = c + (\alpha - 2) \log r_i \qquad (5)$$

The value of $\alpha - 2$ can be estimated as the slope from this linear relationship (Cheng 2007). The standard error and squared correlation coefficient involved in the estimation can be calculated via the fitting method, validated and proposed by least square error method. Also, these indices can be used to evaluate the existence of power-law relationships, Eq. (5). The properties of α and data processing are illustrated in Fig. 1. (Zuo et al. 2009).

2 Study area

Hamyj copper deposit is located in Birjand province, east of Iran. The access road is shown in Fig. 2a. The area chosen for this case study is the Cu porphyry mineralization district. The results of remote sensing and geological surveys show its promising mineralization (Shahi Ferdows et al. 2014). As far as the petrologic field is concerned, this area is composed of volcanic rocks such as the Dacitic volcanic dome, Gabbro, Dacite, Altered Andesite and Andesite and sedimentary rocks such as old Gravel. Gabbro and Andesite Dacite are related to the age of the Cretaceous and Paleogene period, respectively. The geological map is presented in Fig. 2b. The geoelectrical surveying with electrode spacing of 20 m was designed to study and model the mineralization more accurately with more details. Resistivity data have been surveyed by dipole–dipole array. The orientation of two profiles which have been investigated is near N–S. Moreover, maximum depth is around 100 m and ultimately 109 induced polarization data have been studied in this paper.

3 Discussion

Due to the noise in polarization data, the data must be identified accurately and statistically before starting the process. In this paper, this validation was done based on the Doerffel method at 95 % confidence level. Doerffel method identifies outlier data and corrects them based on number and mean of data as well as the related standard deviation. We have written the related cod in Excel software to detect outliers and correct them. After detecting the noise data, polarization data were inversed by Res2MOD software. Inversion of IP data is a two-step process. In the first step, DC resistivity data are inverted to generate background conductivity. By making the assumption that the chargeability, represented by the
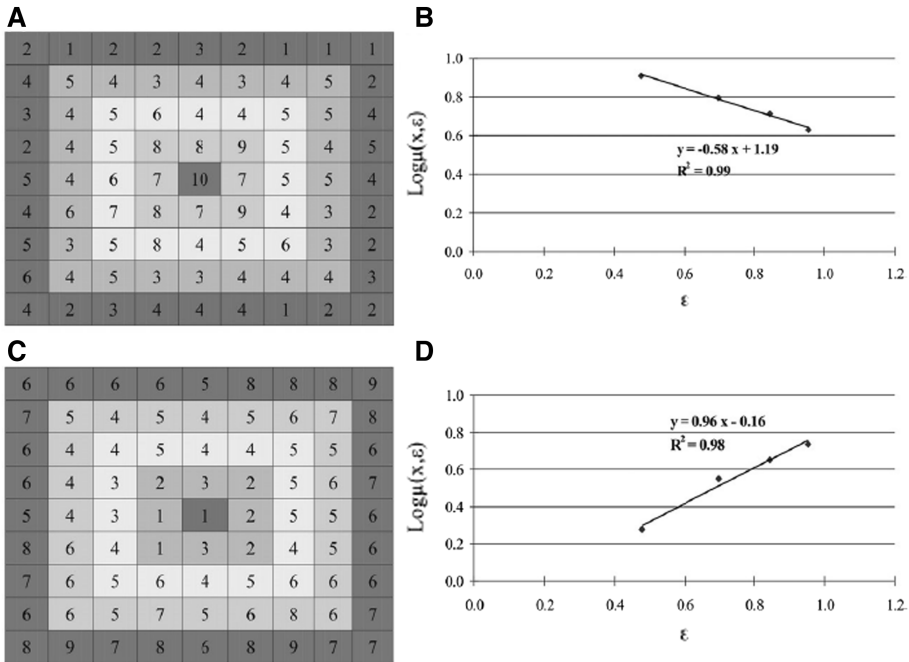
Fig. 1 Illustrations, showing data processing by means of window-based method. **a** and **c** box sizes ranging from 3 × 3, 5 × 5, 7 × 7–9 × 9 were used to estimate the average values resulting from enrichment and depletion of the element concentration values, respectively. **b** and **d** log–log (base 10) plots showing the relationship between the average element concentration values μ (x, ε) and box size ε for **a** and **c**, respectively, with α − 2 estimated from slopes of *straight lines*, that is α = 1.42 < 2 for enrichment pattern (**a**), and α = 2.96 > 2 for depletion pattern (**c**). (Zuo et al. 2009)

symbol μ, are small then the relationship between the apparent and intrinsic chargeability is given by $\mu\_a = J\mu$. In equation J is the element of the sensitivity matrix for DC resistivity problem. The second step of the IP inversion solves a linear inverse problem using equation as the constraints (Oldenburg and Li 1994). Statistical properties of induced polarization data are given in Table 1 and a histogram of data is shown in Fig. 3. Then the following steps were performed on data:

In order to calculate the singularity index, we have written the related code in Matlab software. Singularity index must be calculated for each IP data to classify IP data in anomaly or background class. To calculate singularity index, IP average is calculated in different window size. Window sizes have been considered as 20 m × 3.24 m, 40 m × 10.25 m, 60 m × 17.43 m and 80 m × 25.33 m (window size has been allocated based on the location of inversion data). IP average versus window size has been plotted logarithmically and fitted line has been assigned via least square method. Slop of line has been calculated and singularity index has been identified via Eq. 5. The process has been performed for each IP data until singularity index is evaluated. Statistical properties of the singularity index are given in Table 2 and the Histogram singularity index is shown in Fig. 4.

The singularity map is given on the studied profile in Fig. 5. Based on the singularity index map, plotted by Surfer 12 software, several anomalies in the region are observed
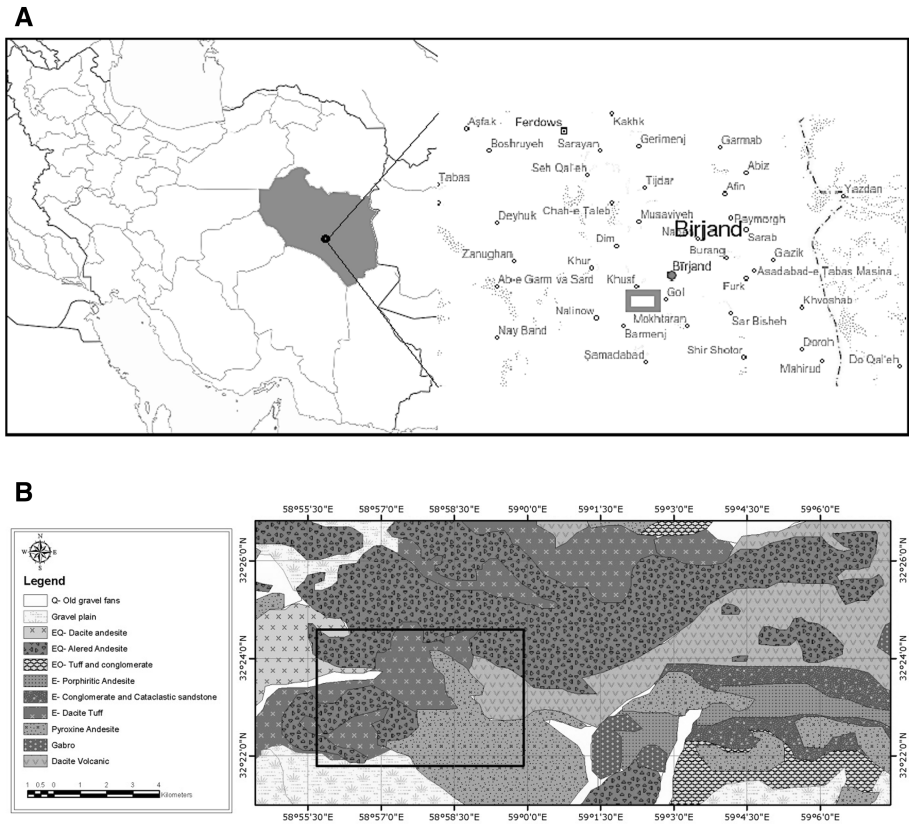
A

B

Fig. 2 a Map of Iran and the studied area **b** Geological map of the region, based on 1:100,000 Birjand geological map

Table 1 Statistical properties of induced polarization data

Number of data	Mean	SD	Max	Min
109	6.63	9.15	50.4	0.001

($\alpha < 2$). All of these areas are located at a depth of 35 m, but with different distances from the beginning of the profiles. The anomalous zones are at distances of 210, 290, 310, 330, 390 and 410 m from the beginning of the profile. Therefore, there are six anomalous data based on Fig. 4.

To calculate the threshold by the concentration-area method, induced polarization data must be classified at the first step to apply this method. Therefore, the data were classified to eight classes according to Sturge's rule. Sturge's rule identifies the number of class based on the number of data. The difference between the upper and lower bound is equal to 6.3 mv/v per class. Since the distance between the electrodes is 20 m, the distance between points is 20 m in the cross section. Therefore, each point covers an area of 20 m × 3.24 m, 20 m × 7.01 m, 20 m × 7.18 m, 20 m × 7.90 m or 20 m × 8.67 m in which the induced
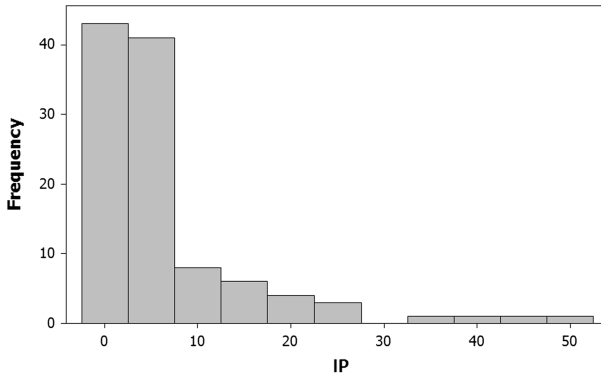
Fig. 3 Histogram of induced polarization

Table 2 Statistical properties of singularity index

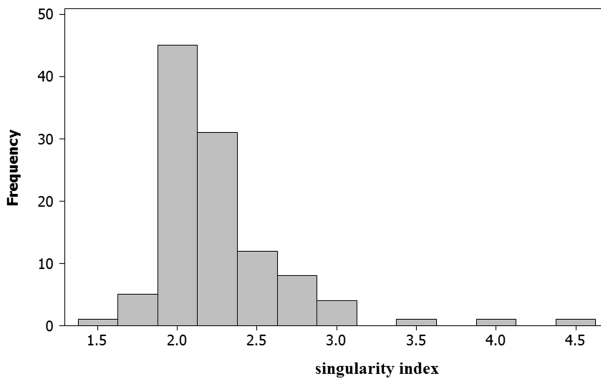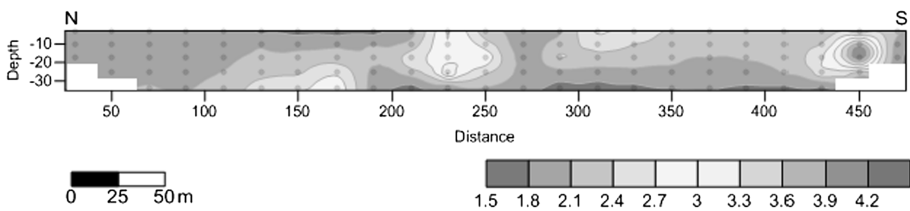| Number of data	Mean	SD	Max	Min
109	2.26	0.4	4.48	1.61

Fig. 4 Histogram of singularity index

Fig. 5 Map of singularity index data

polarization is determined in the center of each cell. One of the sections is presented in Fig. 6.

In the next step, the area of the classified induced polarization should be calculated, (the graphs of all logarithmic is traced so that induced polarization is on the horizontal axis as against the area on the vertical axis) (Fig. 7). Upper bound of the data in this graph have special rule because Doerffel method approve its existence and the number of anomalous data is low. Therefore, this data is must be taken into account for fitting line by least square method.

As is clear from Fig. 7, two lines have been fitted to the reference points by the curve fitting toolbox of Matlab 2012 software (Eqs. 5, 6). In these Equations, R is the correlation coefficient.

$$y = -0.7809x + 3.99 \quad R^2 = 0.8891 \tag{5}$$

$$y = -12.23x + 20.66 \quad R^2 = 0.981 \tag{6}$$

Breakpoint lines indicate the modifications of the population; therefore, breakpoint should be considered as the threshold, because the fractal dimension of anomaly is different from the fractal dimension of the background in the mentioned point. According to Fig. 7, the breakpoint, corresponding to the fractal modification, is determined at about 28 mv/v after back transformation of the logarithmic data.

In Fig. 8, the amount of data and singularity index is shown with respect to each other. Threshold data are specified by the green index and the threshold singularity index is specified by the red index.

According to Fig. 8, there are four regions. Data located in No. 1, have been classified as anomalies by concentration-area while singularity map method cannot recognize it as anomalies since there are no data in this region (region No. 1). Data located in No. 2, has been recognize as background by both concentration-area and singularity map methods since there are many data in this region (region No. 2). Data located in No. 3, has been determined as background via concentration-area; however, singularity map have allocated the data as anomalies since there are two data in this region (region No. 3). Four data [singularity index $(\alpha < 2)$] have been confirmed as anomalies by the concentration-area method. These data are clearly visible in region No. 4. The singularity method and concentration-area method were compared with each other and it was found that 67 % anomalies data corresponded with each other. This may be the reason for the singularity
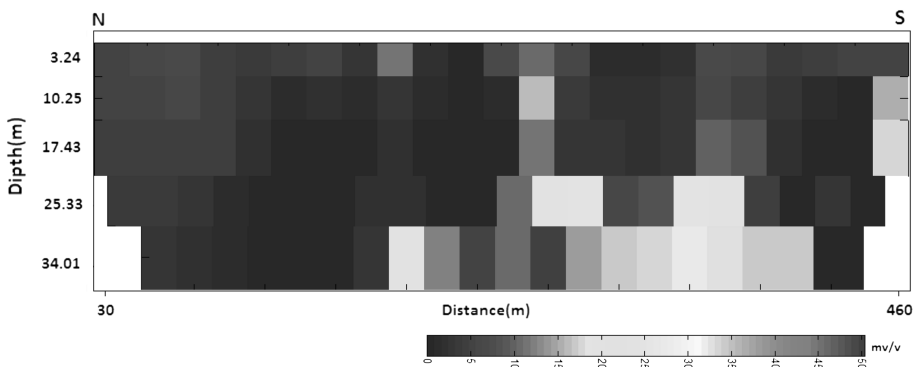

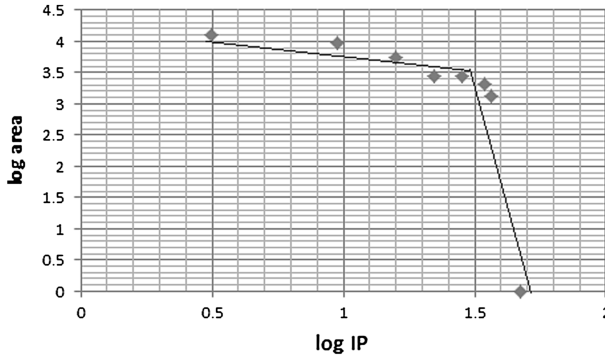**Fig. 6** Cell layout induced polarization data

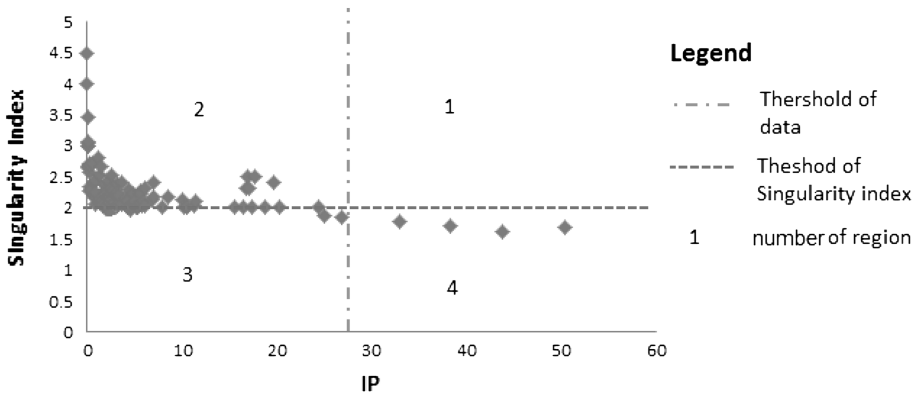**Fig. 7** Graph of logarithmic induced polarization-area

Fig. 8 Scatter plot induced polarization versus singularity index

map to work correctly. All anomaly data (has been recognize by singularity map or concentration-area) located in low resistivity zone.

Data that is located in region No. 4 can propose 1st priority for drilling because two methods approve it. This data is located in depth 35 m and distance 210, 290, 310 and 390 m from the beginning of the profile. Data that is located in No. 3 can propose 2nd priority for drilling because this data is recognized by singularity map method as anomalies and very close is threshold (28 mv/v). This data is located in depth 35 m and distance 330 m and 410 m from the beginning of the profile.

4 Conclusion

In this paper, local anomalies were determined by a spatial statistical method called the singularity map method. Based on this method, the anomalous region (singularity index < 2) is identified in a depth of 35 m and at a distance of 210, 290, 310, 330, 390 and 410 m from the beginning of the profile. Six data have been recognized as anomalies by the singularity map method.

Threshold data is determined by one of fractal methods called the concentration-area method. Threshold data is equal to 28 mv/v. Four data have been recognized as anomalies by this method. Also, the singularity map method is compared with the concentration-area method. Accordingly, 67 % of the anomaly data is confirmed by the concentration-area method. There are two data that the concentration-area has not confirmed as anomalies. According to Fig. 8, there are no data recognized as an anomaly by the concentration-area method and the singularity map cannot recognize them as an anomaly simultaneously. Data that is recognized anomalies by singularity map and concentration-area can be proposed as a priority for drilling. The data is located in depth of 35 m and distance of 210, 290, 310, 390 m from the starting point of the profile. All anomaly data (has been recognize by singularity map or concentration-area) located in low resistivity zone.

Separating anomalies from the background has been developed in the geochemical process and it has currently been expanding rapidly. It is hoped that these methods are also developed in geoelectrical data as well.

References

Bai J, Porwal A, Hart C, Ford A, Yu L (2010) Mapping geochemical singularity using multifractal analysis: Application to anomaly definition on stream sediments data from Funin Sheet, Yunnan China. J Geochem Explor 104(1):1–11

Barton CC, La Pointe PR (1995a) Fractals in petroleum geology and earth processes. Plenum Press, New York, pp 59–72

Barton CC, La Pointe PR (1995b) Fractals in the earth sciences. Plenum Press, New York, pp 77–141

Cheng Q (2006) Singularity-generalized self-similarity-fractal spectrum (3S) model. Earth Sci China Univ Geosci 31:337–348 (in Chinese with English abstract)

Cheng Q (2007) Mapping singularities with stream sediment geochemical data for prediction of undiscovered mineral deposits in Gejiu, Yunnan Province China. Ore Geol Rev 32:314–324

Cheng Q (2008) Non-linear theory and power-law models for information integration and mineral resources quantitative assessments. Math Geol 40:503–532

Dhu T, Dentith MC, Hillis RR (1999) The use of fractal dimension estimators for enhancing airborne magnetic data. Explor Geophys 30(1/2):33–37

Govett GJS, Goodfellow WD, Chapman A, Chork CY (1975) Exploration geochemistry distribution of elements and recognition of anomalie. Math Geol 7(5–6):415–446

Grunsky EC, Agterberg FP (1988) Spatial and multivariate analysis of geochemical data from metavolcanic rocks in the Ben Nevis area. Ontario Math Geol 20(7):825–861

Khalid P, Ghazi S (2013) Discrimination of fizz water and gas reservoir 1 by AVO analysis: a modified approach. Acta Geod et Geophys 48(3):347–361

Mandelbrot BB (1967) How long is the coast of Britain? Statistical self-similarity and fractional dimension. Science 156(3775):636–638

Oldenburg DW, Li Y (1994) Inversion of induced polarization data. Geophysics 59(9):1327–1341

Scholz C, Mandelbrot BB (1992) Special issue on fractals in geology and geophysics. Pure Appl Geophys 131:96–171

Shahi Ferdows M, Bicharanlo Hasan M, Poormirzaee R (2014) Integration of Geoelectrical information layers by fuzzy method to choose the best point for drilling: a case study Hamyj, Birjand. J Earth Space Phys 40(1):95–105 (in Persian)

Sinclair AJ (1974) Selection of thresholds in geochemical data using probability graphs. Geochem Explor 3(2):129–149

Sinclair AJ (1976) Application of probability graphs in mineral exploration. Geochem Explor 4:95

Sinclair AJ (1991) A fundamental approach to threshold estimation in exploration geochemistry: probability plots revisited. Geochem Explor 41(1):1–22

Stanley CR, Sinclair AJ (1989) Comparison of probability plots and gap statistics in the selection of threshold for exploration geochemistry data. Geochem Explor 32(1):355–357

Telford MW, Geldart LP, Sheriff RE (1990) Applied geophysics. Cambridge University, New York, p 726

Xiao F, Chen J, Zhang Z, Wang C, Wu G, Agterberg FP (2012) Singularity mapping and spatially weighted principal component analysis to identify geochemical anomalies associated with Ag and Pb-Zn polymetallic mineralization in Northwest Zhejiang, China. J Geochem Explor 122:90–100

Zuo R, Cheng Q, Agterberg FP, Xia Q (2009) Application of singularity mapping technique to identify local anomalies using stream sediment geochemical data, a case study from Gangdese, Tibet, western China. Geochem Explor 101(3):225–235